PLANAR LAMINAR MIXER

John Evans, Dorian Liepmann, Albert P. Pisano
Berkeley Sensor & Actuator Center, Department of Mechanical Engineering
6117 Etcheverry Hall, University of California, Berkeley, CA 94720-1740

ABSTRACT

Standard approaches to fluid mixing typically rely on turbulence, three-dimensional flows, or mechanical actuators, none of which can be easily implemented in the planar lithographic MEMS design environment. The authors present an approach to mixing for the MEMS environment based on chaotic advection. We outline a design for a device utilizing this approach, verify its theory of operation using numerical modeling, present a fabricated micromixer, demonstrate its ability to move fluid using a thermally actuated bubble-pump, and outline a program of research for further testing and design optimization.

INTRODUCTION

The ability to mix two or more fluids thoroughly and in a reasonable amount of time is fundamental to the creation of fully integrated, "on-chip" micro-electromechanical fluid processing systems. Effective mixing of fluids requires that the fluids be manipulated or directed so that the contact area between the fluids is increased, and the distance over which diffusion must act is decreased to the point that diffusion can complete the mixing process in an acceptable amount of time. In macroscopic devices this is generally done using turbulence, three-dimensional flow structures, or mechanical actuators. As MEMS devices are fabricated in a planar, lithographic environment, design constraints mitigate against mechanical actuators or three-dimensional flow structures.

The size and proportions of MEMS devices generally preclude relying on either turbulence or diffusion alone as mixing mechanisms. The size of fluid chambers in a MEMS device can range from the picoliter, $(10\ \mu m)^3$, to the microliter, mm^3, range. Through fabrication constraints allow for picoliter chambers, few commonly used fluids are concentrated enough to be useful in such quantities. An upper bound on volumes of about 50 μl is set by the size of a typical device (10 mm x 10 mm x 500 μm). Process volumes in the 100 nanoliter range allow multiple chambers to be fabricated on one die, yet provide sufficient fluid for many applications.

Turbulence occurs in flows characterized by high Reynolds numbers, defined as

$$\mathrm{Re} = (U\delta)/\nu\,, \qquad [1]$$

where U is a characteristic velocity, δ is a length scale, and ν is the kinematic viscosity (1 mm^2/s for water). The appropriate length scale, typically the channel height, will in general be smaller than 500 μm. Assuming the highest velocity to be experienced for on-chip flows is one die length per second (U=10 mm/s), we find an upper bound on the Reynolds number of $\mathrm{Re} = 5$, with typical values being much lower. As turbulence in channel flow occurs only for $\mathrm{Re} > 2000$, we expect on-chip flows to be laminar, and we can discount turbulence as an available mixing mechanism. Moreover, flows with $\mathrm{Re} \ll 1$, known as creeping flows, are symmetric and reversible. In this regime, a flow moving past an object will reconstitute itself, passing by the object unchanged, and "mixing" caused by a given set of manipulations to the fluid can be undone simply by reversing the set of manipulations. This precludes the use of barrier-fields, complex geometries, and severely limits the usefulness of mechanical actuators.

Similarly, the size and shape of MEMS devices limit the usefulness of diffusion as a sole mechanism for mixing. As it is difficult to place two fluids one on top of the other in a planar MEMS device, the length over which diffusion must act will be the in-plane dimension of the fluid chamber. Using Fick's equation, a diffusion mixing time scale, T_D can be formed

$$T_D = L^2/k\,, \qquad [2]$$

where L is the relevant mixing length, and k is the Fickian diffusion constant ($k = 10^3\ \mu m^2/s$ for salt in water, for example). Using L = 1 mm, we find $T_D = 10^3$ seconds = 16.6 minutes. Even for L = 100 μm, T_D = 10 seconds. Such mixing times are generally too slow to rely on diffusion for effective mixing.

0-7803-3744-1/97/$5.00 © 1997 IEEE

PULSED DIPOLE MIXER

Chaotic Advection

The device presented here employs chaotic advection to mix fluids in a planar, laminar environment. A chaotic flow field is one in which the path and final position of a particles placed within the field are extremely sensitive to their initial position. In a chaotic flow field, particles initially close together may become widely separated, and the flow as a whole becomes well mixed. A laminar flow field is one in which velocity, pressure, and other flow parameters do not vary irregularly with time. Chaotic advection is the process of mixing using flow fields that are entirely regular in space and time, yet which cause particles initially close together, to become widely separated, and the flow as a whole well mixed.

Mixer Design

Theoretical work by Jones and Aref (1988) has shown that the purely two dimensional flow consisting of blinking spatially separated sources and sinks is a chaotic system. A particle in such a flow moves alternately away from the source, and then towards the sink, with fluid injested by the sink being expelled by the source.

In an enclosed, finite device, sources and sinks must occur in pairs to satisfy mass conservation. The anti-mymmetric first-in-last-out pulsed finite-dipole mixer is arguably the next simplest configuration and consists of two source/sink sets arranged antisymmetrically. Figure I is a photograph looking into a fabricated pulsed dipole mixer through its quartz coverplate. Dark regions are 100 μm deep trenches etched in a silicon wafer. The central “pill shaped” mixing chamber is flanked by four channels. The upper-left and lower-right are sources (inputs), while the lower-left and upper-right are sinks (outputs). These channels lead through check-valves to circular piston-type pumping chambers. In operation, fluids to be mixed are loaded into the mixing chamber, and pumps and valves are activated so as to move fluid repeatedly left-to-right across the top (upper dipole), then right-to-left across the bottom (lower dipole), with plugs of fluid extracted by a sink being inverted before reinsertion by a source (first-in-last-out). This implementation utilizes thermally created vapor bubbles for both pumping and valves, with heat supplied by polysilicon heaters and aluminum traces (shown), both fabricated on the quartz coverplate. However, the mixing process presented here is independent of pump and valve technology.

The pulsed dipole mixer is characterized by a source/sink separation distance for each dipole, 2*a*; a dipole/dipole separation distance, 2*b*; and a source/sink strength (see Figure I). As is common in fluid mechanics, the source/sink strength is specified by *Q* (area per second), such that the volume (expressed as an area) that each source and sink pumps into an infinite plane in each stroke is Qt, where t is the length of time that each source/sink operates. In the enclosed prototype device, each source/sink expels fluid into a half-plane, and thus the pump size is decreased to $V = (Qt)/2$. As shown in Figure I, we can also characterize the pump size by a length scale λ, where $\lambda = \sqrt{(Qt)/\pi} = \sqrt{(2V)/\pi}$.

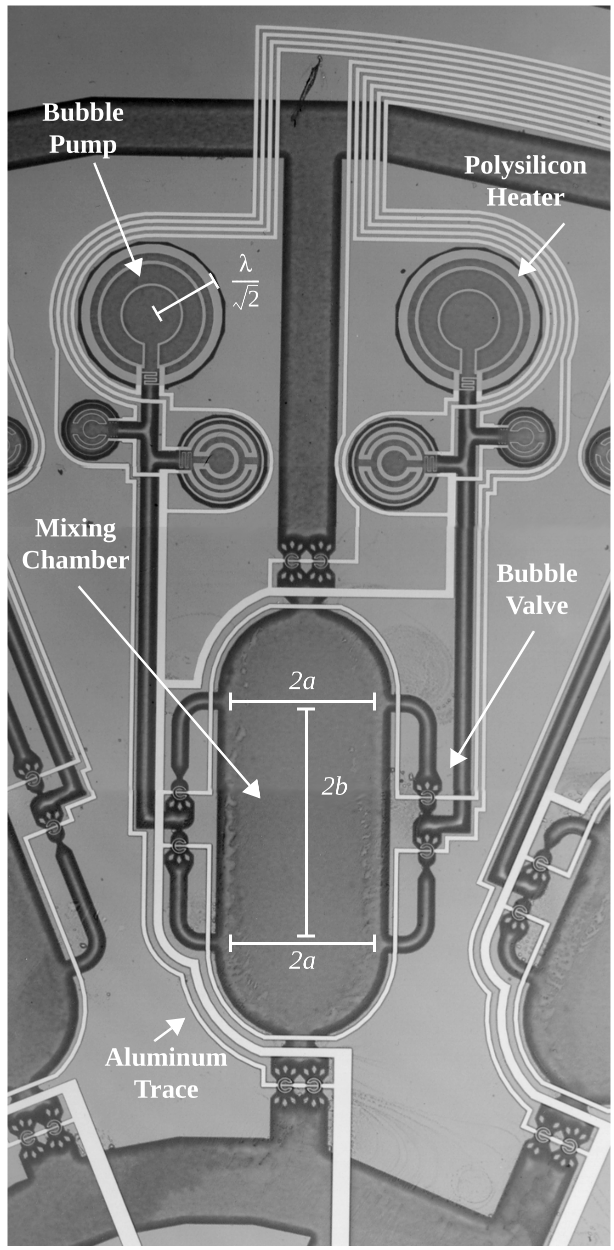

FIGURE I. Photograph looking into a fabricated microfluidic mixer through its quartz coverplate. B=*1.5,* a = *300* μ*m,* b = *450* μ*m, and* $\lambda/(\sqrt{2})$ = *106* μ*m, 159* μ*m, and 254* μ*m.*

Ignoring viscosity, diffusion, and the height of the device, we now have three length scales (a, b, and λ), which define a two parameter system: B=b/a, the aspect ratio of the mixer, and $\Lambda = \lambda/a$, the relative pump size. Extreme values of these parameters yield devices which, in general, produce little mixing. For example, for large aspect ratios, B, the two dipoles will be widely separated and will operate independently, creating a net clockwise flow, but little mixing. For small aspect ratios, the upper and lower dipoles will be nearly on top of each other, and will simply undo each other's work. Similarly, for small pump sizes, Λ, the time dependence is effectively lost and the flow will approach a steady quadrapole flow. Finally, for large pump sizes, Λ, the ratio of fluid in the pump to that in the mixer will become large, and the effect of the mixer itself will be negligible. Though plug inversion caused by the first-in-last-out pumps creates additional complications (which we will not examine here), analysis of limit cases leads us to expect that optimal mixing will occur for over a range of moderate pump sizes and aspect ratios.

Fluid Flow

The Navier-Stokes equations can be solved numerically to predict the laminar flow field within an arbitrary device, but such modeling is beyond the scope of this study. Instead, the authors consider the case of quasi-steady, incompressible flow where the depth of the fluid channels and chambers (δ) is much less than their in-plane size (L). Quasi-steady, incompressible flow with $\delta/L \ll 1$, and $\mathrm{Re} \ll (\delta/L)$ is dominated by a viscosity-pressure balance, and is known as Hele-Shaw flow.

Though the flow in a pulsed system is inherently time-dependent, we may consider the flow effectively steady if the effects of temporal acceleration are negligible compared to both viscous effects and convective acceleration effects. Two indicators may be used to justify the quasi-steady flow approximation. First, viscous effects dominate over temporal acceleration effects if $(\delta^2 f)/\nu \ll 1$, where f represents the device operation frequency (dipole alternation frequency), δ is the viscous length scale (chamber height), and ν is the fluid kinematic viscosity. Assuming a cycle frequency of one Hertz, and a chamber height of 100 µm yields $10^{-2} \ll 1$. Second, viscous effects exceed convective acceleration for small Strouhal numbers $\mathrm{St} = (Lf)/U \ll 1$, where L is the in-plane flow dimension.

Similarly, the flow is said to be incompressible if $\mathrm{Ma}^2 \ll \mathrm{Re}_L$, where $\mathrm{Ma}=\mathrm{U}/c$ is the standard Mach number, and $\mathrm{Re}_L = (\rho UL)/\mu$ is Reynolds number based on the in-plane flow scale, L. Note that this is a less restrictive criteria than the standard incompressibility requirement $\mathrm{Ma}^2 \ll 1$.

For steady-incompressible Hele-Shaw flow, the flow profile is given by

$$\vec{u}(x, y, z) = \frac{1}{2\mu}(a^2 - z^2)\nabla P(x, y)\,, \qquad [3]$$

where $\vec{u}$ is the fluid velocity, a is the chamber half height, ∇P is the pressure gradient in the horizontal directions, and x, y, and z are, respectively, the two horizontal and one vertical coordinates. Within each horizontal plane the flow field is given by potential flow theory, where the pressure serves as the potential. In the vertical direction, the flow is parabolic, with zero flow at the tops and bottoms of the chambers. Note that the viscous no-slip boundary condition is not discarded at the walls, rather, the "boundary layer" at the walls will be thin, of order δ, and can thus be neglected.

The fluid flow through the prototype device can then be computed numerically using a relaxation method. Streamlines for the case B=b/a=2 with the upper dipole in operation are shown in Figure II. Note that the shape of the flow field is independent of both the pump size and the vertical plane under-consideration. Given a pump size, the average velocity at any horizontal point, $\bar{u}$, can be predicted using the stream function of Figure II. The velocity at any vertical position can then be computed noting

$$\frac{u(x, y, z)}{\bar{u}(x, y)} = \frac{3}{2}\left(1 - \frac{z^2}{a^2}\right). \qquad [4]$$

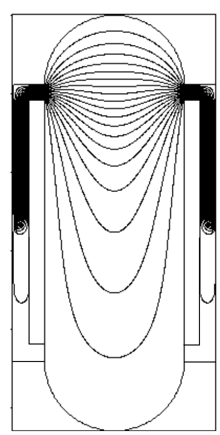

FIGURE II. Numerically computed streamlines within an idealized device with the upper dipole activated and lower dipole inactive. B=2.

NUMERICAL MODELING

Examination of extreme values for the two parameters in the pulsed double-dipole system indicates moderate values of aspect ratio, B, and pump size, Λ, will produce the best mixing. Research is underway to determine the optimum combination of values, both experimentally and numerically. The numerical model assumes steady, incompressible, Hele-Shaw flow, and operates by solving for the stream function within an idealized device using a relaxation method, computing the height averaged flow field, seeding half of the device with about 2500 markers, and then, assuming no diffusion, tracing the movement of these markers during device operation. Tracer positions after 0, 6, 12, and 18 operations of both the upper and lower dipoles (i.e. cycles) are shown on the right in Figure III for the case B=2, Λ= 0.75.

To assess the quality of the mixing at each step and for each mixer design, a mixing index is formed by dividing the mixer into $N \approx 100$ sections (of roughly equal area), computing the particle concentration in each section ρ_i, the area of each section A_i, and the averages of both numbers (denoted by overbars), and then computing

$$\text{Mixing Index} = \sqrt{\frac{1}{N}\sum\left(\frac{A_i}{\bar{A}}\right)\left(\frac{\rho_i-\bar{\rho}}{\bar{\rho}}\right)^2}, \qquad [5]$$

which is the area weighted standard deviation of the concentrations divided by the average concentration. Model results after 0, 6, 12 and 18 cycles are shown in Figure III (left) for a range of aspect ratios, B, and pump sizes, Λ. The mixing index is unity for a volume half-full of uniformly distributed tracers. At cycle zero, each mixing chamber is half-filled with tracers and half-filled with clear fluid. However, pipes, valves, and one set of pumps are also filled with clear fluid. Thus, the device as a whole is less than half-full of tracers, inflating the starting mixing index. The mixing index for perfectly mixed fluid is theoretically zero. However, in practice, using a finite number of tracers and dividing the mixer into a finite number of regions yields a larger number for the perfectly mixed case. For the cases shown, perfect mixing occurs at 0.2. The results show best mixing occurs for devices in the neighborhood of B=2, Λ=0.75 (shown on right).

These data serve as a conservative design model for mixing in the device, as they discount mixing generated by the parabolic vertical flow profile (advection), and that caused by vertical and horizontal diffusion. Future research will consider alternate loading scenarios, as well as these additional mixing mechanisms.

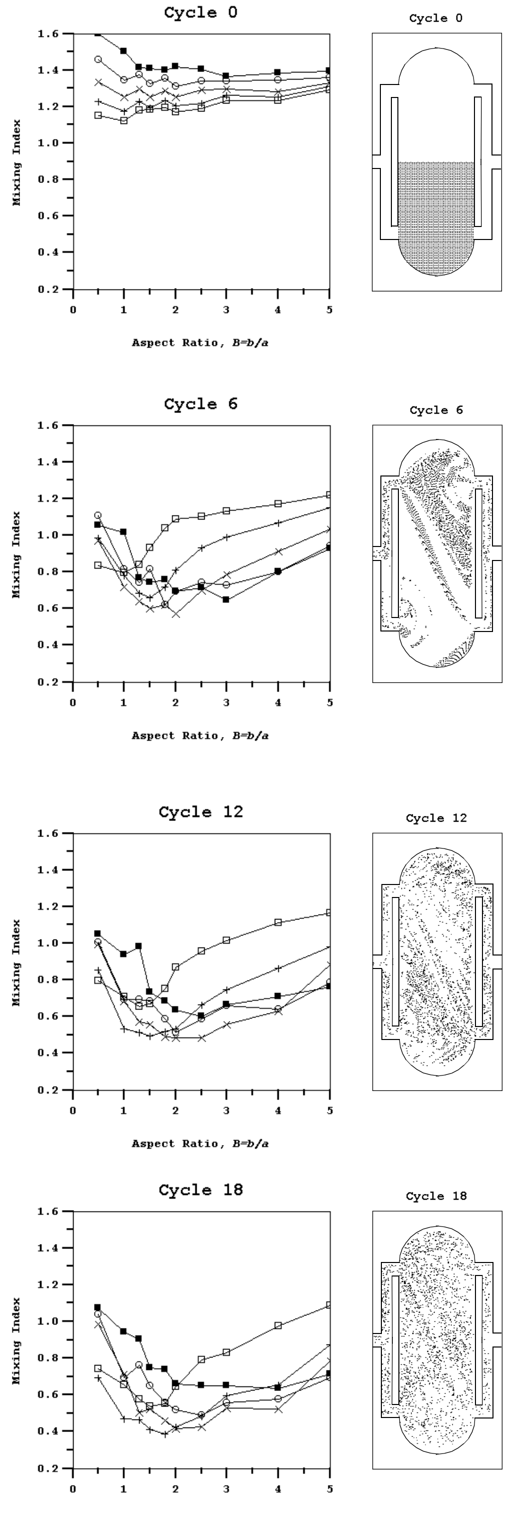

FIGURE III. Numerically computed mixing index for a range of aspect ratios, B=b/a, *and pump sizes,* $\Lambda=\lambda/a$ *(left); and particle positions for the case* B*=2,* Λ*=0.75 (right), both after 0, 6, 12, and 18 cycles. On the left, values for* $\Lambda=\lambda/a$ *are: open box = 0.5, cross = 0.75, x=1.00, circle=1.25, closed box=1.5.*

EXPERIMENTAL PROGRAM

Overview

A fully integrated, multi-component prototype device has been fabricated. An annotated layout of the ten millimeter die is shown in Figure IV. The device incorporates five mixing chambers, 37 bubble pumps, 48 thermo-capillary bubble valves, 3 input/output ports, and ducts of various dimensions. The five mixing chambers have aspect ratios, *B*, ranging from 1 to 3.5. Each is fitted with three pumps on each side, with radii $\lambda/(\sqrt{2}) = 106\ \mu m$, 159 µm, and 254 µm, which can be operated alone or jointly in up to seven different permutations, yielding seven effective pump sizes for each chamber. Thus, the device incorporates 35 effective permutations of aspect ratios and pump sizes which bracket the range of optimal mixing predicted numerically.

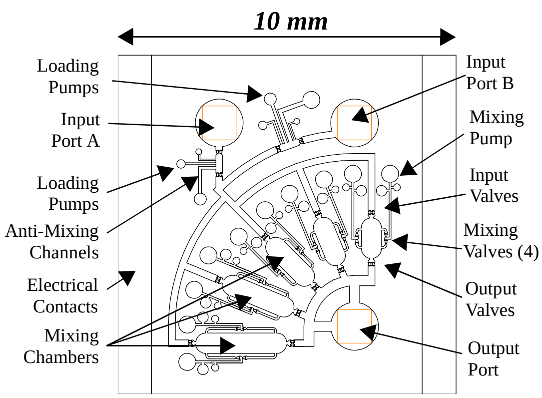

FIGURE IV. Die layout for fabricated 1 cm^2 test device. Channels shown are etched into silicon wafers.

A photograph of one of the five mixing chambers (the second from the right) is shown in Figure I, and has been previously described.

Fabrication

These devices are fabricated at the Berkeley Microfabrication Facility using a five mask process. An abbreviated process flow is shown in Figure V. Flow channels, pumping chambers, valves, and electrical contact zones were etched 100 µm into a silicon substrate by Surface Technologies Systems (STS), forming the required channel geometries. This depth was chosen due to fortuitous access to the STS etching technology. A shallower depth would be more consistent with the Hele-Shaw approximation and would yield better agreement with numerical models. Fluid access ports are created by depositing and patterning a protective nitride layer, and then etching

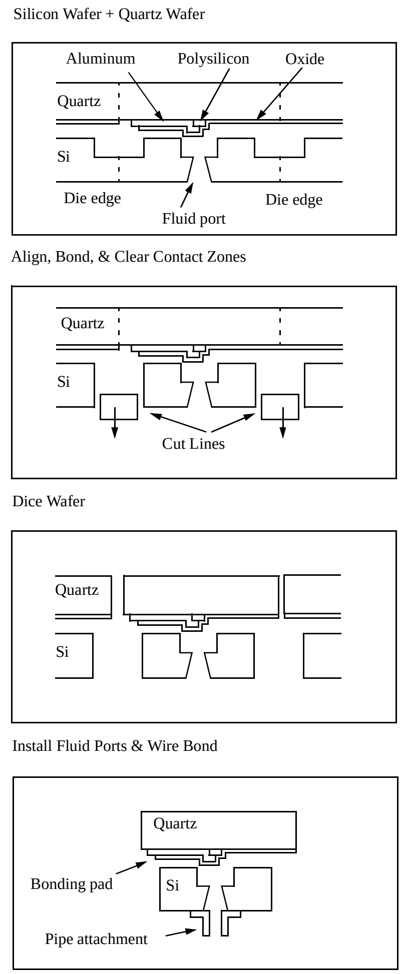

FIGURE V. Abbreviated process flow for micromixer fabrication.

through-holes into the silicon wafer using an anisotropic KOH etch.

Polysilicon heaters and aluminum electrical traces are defined on quartz wafers, and encapsulated within an oxide layer. The oxide layer is then etched to reveal bonding pads, and the silicon and quartz wafers are aligned, bonded, and diced, resulting in stand-alone devices one millimeter thick, and ten millimeters square.

Bubble-Valves

Thermo-capillary bubble valves operate by creating a vapor bubble within specially designed chambers and then using these bubbles prevent flow through the chamber. A bubble can support a pressure differential if the radii of curvature, *r*, of its front and rear surfaces differ. The magnitude of this pressure differential is $\Delta P = \sigma(1/r_1 - 1/r_2)$, where σ is the surface tension

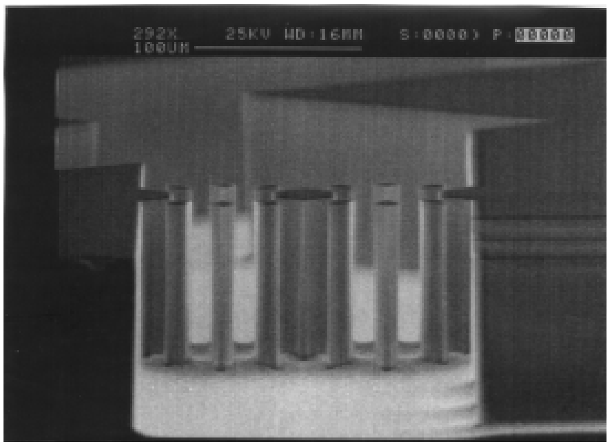

IGURE VI. Scanning Electron Micrograph (SEM) of wo bi-directional bubble valves.

(around 0.6 atm-μm for water). By splitting the front interface into a set of parallel converging passages, and using a single parallel, or curricularly converging, rear passage, the difference between the two radii can be increased. (Note that for chambers with a constant height, only the in-plane radii are significant.)

These principles motivate the design of bubble check valves (shown to the left and right of the mixer in Figure I), and the bi-directional bubble-valve (shown above and below the mixer in Figure I). A scanning electron micrograph (SEM) of a bi-directional valve is also shown in Figure VI. Diamond shaped columns, 13 μm wide and 100 μm tall form a cage which constrains bubble movement. The valve is designed to withstand a pressure differential on the order of 0.05 atm, about and order of magnitude larger than required for a 0.5 Hz mixing cycle frequency.

Bubble-pumps

Bubble pumps, shown in Figure I, operate by thermally creating bubbles within circular chambers, thus effecting a volume expansion, and a piston-type action. Figure VII shows one pump in action. The left image shows the upper pump on the left side turned off. (The small bubble in the chamber is a residual air bubble left over from before the device was filled with liquid.) Note the presence of a tracer bubble in the long fluid channel on the left. In the right photo, this pump has been activated, and is now filled with a steam bubble. The tracer bubble has moved about 520 μm, indicating a displacement of about 3.1 nl. This displacement will increase as the filling process is perfected, and the residual bubble removed.

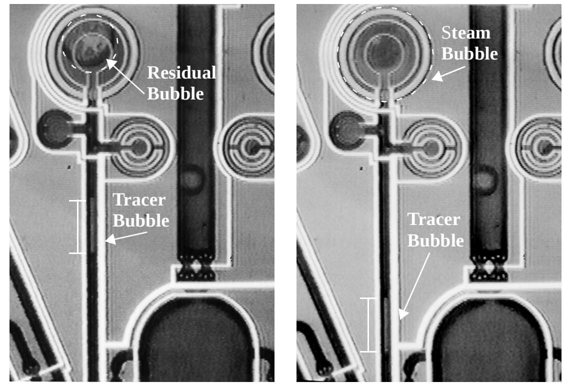

FIGURE VII. Photographs of bubble-pump in operation. Tracer bubble has moved 520 μm, indicating a displacement of about 3.1 nanoliters.

Project status and future work

The micromixers presented are currently undergoing component and system level testing. After testing is completed, mixing runs will be conducted for each of the 35 combinations of aspect ratio, *B*, and pump size, Λ, and these runs compared with numerical predictions. Additionally, Digital Particle Image Velocimetry (DPIV) will be employed to measure the flow field within the device for comparison with theory.

CONCLUSIONS

The authors present an approach to mixing in a planar, laminar, MEMS environment based on chaotic advection; outline a design for a device utilizing this approach; verify its theory of operation using numerical modeling; present a fabricated micromixer; demonstrate their ability to move fluid within the device using a bubble-pump; and outline a program of research for further testing and optimization.

ACKNOWLEDGEMENTS

The authors would like to thank Becton Dickinson and Company, and the Berkeley Sensor & Actuator Center for their financial support. Additionally, the authors would like to thank Ajay Deshmukh and Tori Bailey for their assistance with the numerical investigation presented in Figure III; and the staff of the Berkeley Microfabrication Facility and Surface Technologies Systems Limited (Prince of Wales Industrial Estate, Abercarn, Newport, Gwent NP1 5AR, UK, Tel: +44 1495 249044) for fabrication assistance.

REFERENCES

Jones, S. and Aref, H. (1988), "Chaotic advection in pulsed source-sink systems", Physics of Fluids, **31**: 469-85.